Adhesive Gold Nanoparticles for Easy and Controlled Surface Coating

Tianchi Liu,[†] Fan Yang,[‡] Xing Wang,[§] and Jun Feng Liang[†],*

[†]Department of Chemistry and Chemical Biology, Schaefer School of Engineering and Science, Stevens Institute of Technology, Hoboken, New Jersey 07030, United States

[‡]Department of Chemical Engineering and Materials Science, Stevens Institute of Technology, Hoboken, New Jersey 07030, United States

[§]Beijing Laboratory of Biomedical Materials, Beijing University of Chemical Technology, Beijing 100029, PR China

ABSTRACT: Gold nanoparticles (Au NPs) are one of the most important nanomaterials due to their unique properties and broad applications. Among these applications, decorating Au NPs on universal surfaces is highly desired. Herein, we report adhesive Au NPs functionalized by borated dopamine dithiocarbamate. Such Au NPs are nonreactive in colloidal solution but can be activated at an acidic pH to produce adhesive Au NPs and initiate spontaneous surface coating through deprotected catechol-mediated reactions. Easy and controllable surface coating was achieved on materials with distinguished chemical and physical properties because of the high reactivity of catechol. Adhesive Au NPs represent new surface coating method with wide application potentials.
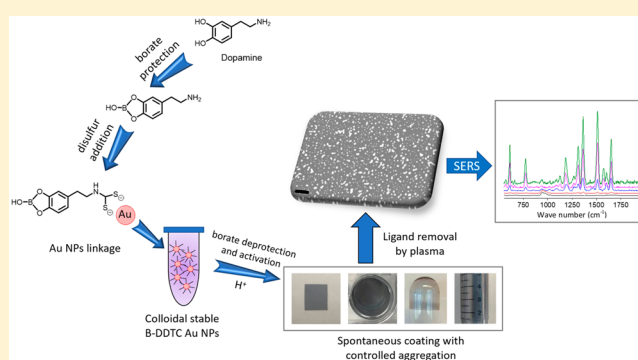
INTRODUCTION

Nanoparticles can be defined as particles with a diameter of 1−100 nm, and recent research on nanoscale particles has presented very promising applications due to their unique properties. Among them, gold nanoparticles (Au NPs) are one of the most extensively investigated areas. As a reasonably inert metal, gold does not oxidize at temperatures below its melting point, and it does not react with most of the chemicals. More importantly, due to their unique tunable optical properties, Au NPs can be applied to various applications such as sensing, detecting, and imaging in biosensing areas.[1−3] For example, the gold nanoparticles can be used to enhance both Rayleigh and Raman signals to obtain chemical information on many biological species of interest, which were previously unattainable using simple spectroscopy setting.[4−6] Au NPs represent an excellent nano platform in developing analytical methods for wide biosensing applications, surface enhanced Raman scattering (SERS) spectroscopy in particular,[7−9] and targeting chemical and biological samples.[10−13]

With continuously evolving synthesis techniques, great improvements have been made in the control over Au NP size and shape[14] and intended optical properties.[11] Commonly, synthesis of Au NPs is conducted either in aqueous or organic solvents. To further functionalize material surfaces with Au NPs, nanoparticle immobilization is always required. However, there are still challenges and difficulties to overcome. Functional surfaces are traditionally prepared by physical deposition of the nanoparticles on substrates. Some researchers also have reported seeding methods with particle growing pathways.[15]

During the nanoparticle immobilization process on the substrates, substrate surfaces usually require either physical or chemical pretreatment. Moreover, various chemicals are involved in controlling aggregation and improving the distribution of the nanoparticles for good sensing properties. These assistant chemicals are usually removed for future sensing applications through hours of thermo-treatment to eliminate possible chemical signal noise. All these steps undoubtedly increase processing time and complexity.

In this research, we developed a new approach to synthesize colloidal stable adhesive Au NPs, which can be quickly and easily immobilized on material surfaces with even and controllable distribution. (Figure 1). We chose to anchor borate protected dopamine dithiocarbamate (B-DDTC) on Au NPs, leading to colloidal stable adhesive Au NPs for easy immobilization on universal surfaces without any surface pretreatment. Dopamine is a small molecule that mimics the adhesive component, L-DOPA, of marine mussels with the chemical structure of catecholamine.[16] Under alkaline conditions, the catechol functional group oxidizes to quinone allowing dopamine to self-polymerize and form a thin film of support on surfaces through covalent bonding and other strong intermolecular interactions including hydrogen-bonding, metal chelation, and π−π interactions.[17,18] We utilized this adhesive property to achieve the immobilization of gold nanoparticles by a simple
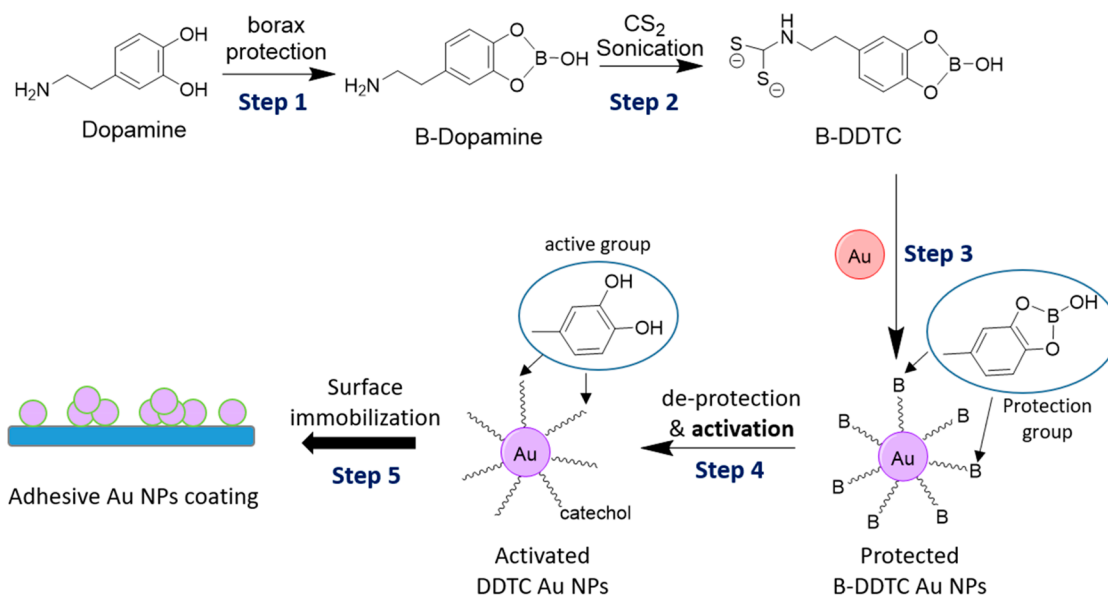
Figure 1. Scheme of step-by-step synthesis of B-capped DDTC-Au NPs and spontaneous surface coating of adhesive Au NPs. Step 1, borate protection of dopamine molecule; step 2, disulfur bond addition to B-dopamine molecule to create ligand linkable to Au NP surface; step 3, ligand linkage with premade Au NPs to synthesize protected B-DDTC Au NPs which are stable in colloidal solution; step 4, activation of adhesive Au NPs through deprotection of borate in acidic pH for surface immobilization; step 5, surface coating process of adhesive Au NPs on surfaces.

step, and particle aggregation was controlled by introducing borate protection before immobilization.

EXPERIMENTAL SECTION

Synthesis of B-DDTC-Au NPs. Au NPs were synthesized from gold(III) chloride ($HAuCl_4$) using sodium borohydride ($NaBH_4$) as the reducing agent. Briefly, 11 mL of 0.01 M of $HAuCl_4$ (0.011 mmol) in Milli Q water was prepared, then 0.627 mg $NaBH_4$ (0.0166 mmol) was weighed and made into a 600 μL aqueous solution (in 1.5 mL EP tube) with Milli Q water. The newly prepared $NaBH_4$ solution was drop-added into $HAuCl_4$ (aqueous) under vigorous stirring for 2 min. The light-yellow solution then turned into a wine-red color, and the Au NPs were obtained. Second, we weighed 26.15 mg of dopamine monohydrochloride (0.1376 mmol) and dissolved it in 1.5 mL of borate buffer (0.1 M $Na_2B_4O_7 \cdot 10H_2O$, 50 mM NaOH, 0.1 M NaCl), the reaction mixture was then sonicated for 5 min. After that, 10 μL of CS_2 was added, and the mixture was sonicated for another 5 min. The 1.5 ml of borated protected dopamine dithiocarbamate (B-DDTC) function-alized dopamine solution was added to a 10 ml portion of previously prepared Au NPs solution, and the mixture was stirred at room temperature for 15 min to produce B-DDTC-Au NPs. All chemicals are purchased from Sigma-Aldrich.

Three precursor compounds were freeze-dried and then charac-terized through nuclear magnetic resonance spectroscopy (NMR), Fourier-transform infrared spectroscopy (FTIR), and UV−vis spec-troscopy. Hydrodynamic particle radii were measured through a dynamic light scattering (DLS) system using MALVERN Zeta sizer Nano ZS device. FTIR spectra were performed with a Bruker Tensor 27. We collected the spectra by averaging results of 128 scans at 2 cm^{-1} resolution ranging from 4000 to 600 cm^{-1}. All samples were prepared into a pellet with KBr. The chemical structures were investigated by ^{1}H NMR using a Bruker AVANCE 500 spectrometer. Three NMR samples were prepared in deuterium oxide (D_2O) as a solvent. All spectra were measured at 303 K.

Adhesive Au NPs Activation and Universal Surface Coating. The crude B-DDTC-Au NPs were activated through washing with pH 3 Milli Q water (adjusted with HCl) to remove the borate protection. After centrifugation, DDTC-Au NPs were washed twice using pH 3 water and water/ethanol (3:7) solution to obtain the activated DDTC-Au NPs. Then the surface coating using adhesive DDTC-Au NPs was conducted on various materials, including polystyrene (PS), poly-

ethylene terephthalate (PET), polypropylene (PP), and glass (borosilicate). Materials were immersed into 5 mM/Au DDTC-Au NPs H_2O/EtOH mixture (water/ethanol = 3:7) for up to 24 h and then dried in air. DDTC-Au NP coated surfaces were prepared. Samples were then treated with oxygen plasma at a power of 80 W for 1 min to exclude the dopamine residue on the surfaces. Scanning electron microscopy (SEM) images of DDTC-Au NP coated silicon wafer samples were studied with Zeiss Auriga small dual-beam FIB-SEM at an accelerating voltage of 5 kV. After the coating process, the dried samples were gently rinsed with Milli Q water to remove the free particles. Before the samples were loaded for SEM, the surface was dried in air to eliminate free particles. The gold spin coating was not required. The stabilities of DDTC-Au NP coated surfaces were tested in different pH and salt solutions for 24 h incubation periods.

Au NP Aggregation and SERS Effect. Raman spectroscopic measurements were performed using a custom-built setup. A 632.8 nm wavelength laser beam was spatially filtered and reflected from a Chroma Z633RDC dichroic mirror which exited the back aperture of a Thorlabs 20 × 0.55 N.A. objective. The excitation laser intensity in front of the objective was 8 mW. The sample was placed on a Newport ULTRAlign 561D translation stage. A fiber-coupled Acton Spectra Pro 2300 spectrometer with a Roper Scientific liquid nitrogen cooled CCD detector was used in spectrum acquisition. The objective was used to produce a large laser-focusing beam (~1 mm in diameter). All Raman measurements were performed using an acquisition time of 20 s (exposure time of 2 s × 10 integral exposures).

RESULTS AND DISCUSSION

Synthesis of Functionalized Au NPs and Character-izations. The first two steps of chemical synthesis (Figure 1) was confirmed by NMR, FTIR, and UV−vis spectroscopy analyses. In the ^{1}H NMR spectrum (Figure 2a), aromatic hydrogens were numbered with 1, 2, and 3. Compared with pure dopamine, all three aromatic hydrogens decreased in chemical shift. Dual doublets peaks at 6.68 and 6.66 ppm belong to hydrogen 1 due to proton−proton coupling (CH−C) that was shifted to high field with a decrease to 6.51 and 6.49 ppm; the 6.76 ppm doublet peak belongs to hydrogen 2 and decreased to 6.53 ppm (C−CH); the 6.82 ppm doublet peak belongs to hydrogen (3) which decreased to 6.56 ppm.[19,20] After
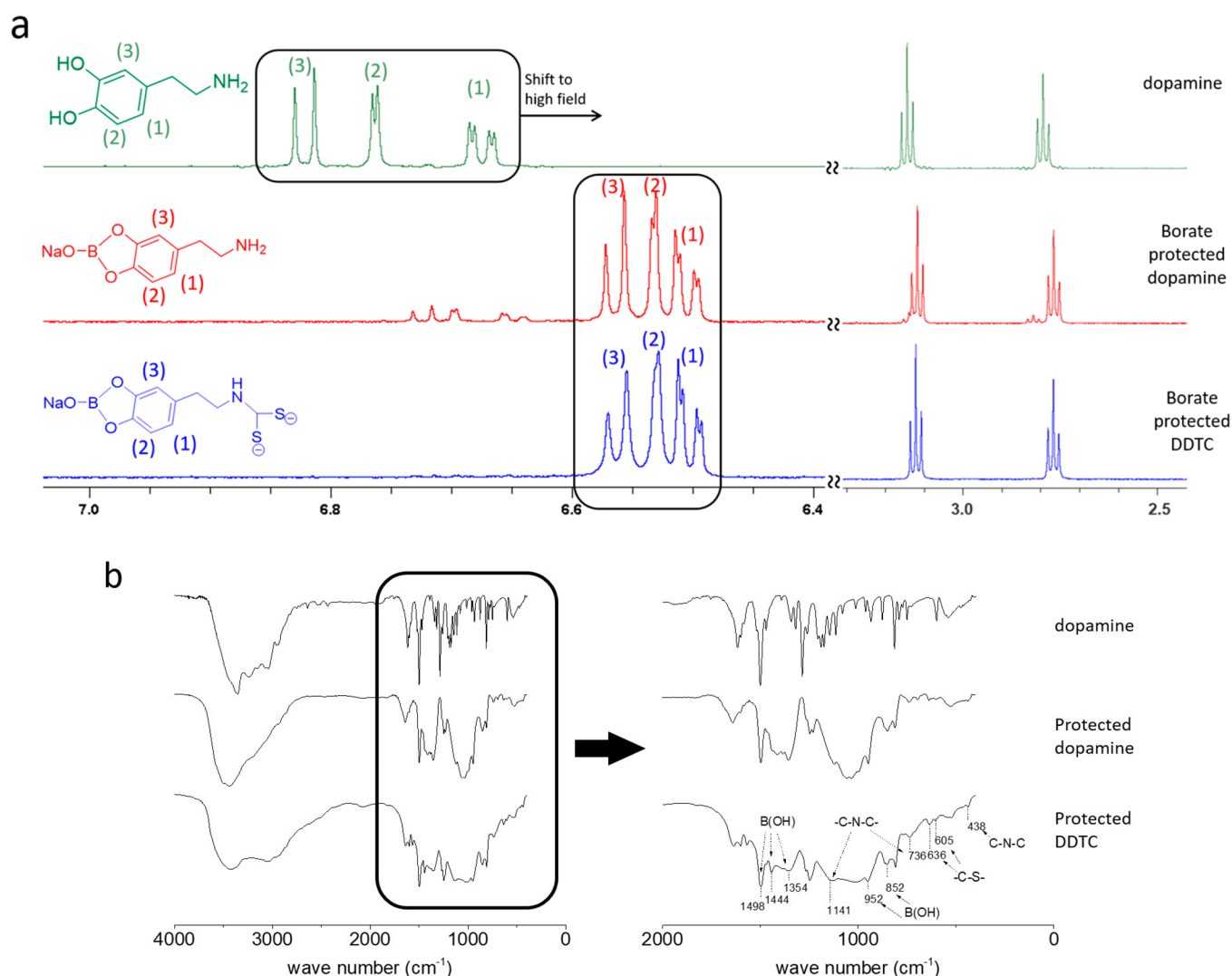
Figure 2. (a) NMR spectra comparison of the three precursor compounds: dopamine, borate protected dopamine, and borate protected DDTC. (b) FTIR spectra of dopamine, dopamine protected with borate, and dithiocarbamate addition.

temporary protection with borate, which can easily deprotect in acidic condition,[21] the newly formed five-membered heterocyclic structure increased the electron density contribution to the molecule compared with the two−OH groups (phenol). As a result, all the chemical shifts of the aromatic hydrogens shifted to the higher field (lower ppm). The evidence can be found in the ^{1}H NMR spectra comparison of the three compounds (Figure 2a). Also, the peaks of hydrogens on the aliphatic carbon chain (−CH₂−CH₂−) and the two triplets at 3.14 and 2.79 ppm were presented on the spectrum.[22,23] However, the aliphatic hydrogen barely had a distinct change (from 3.14 to 3.12 ppm, and from 2.79 to 2.76 ppm) due to the aliphatic hydrogen being too far away from the changed electron contribution. There was no clear sign of dopamine polymerizations, proving the borate protection.

FTIR spectra shown in Figure 2b indicates the functionalized Au NP ligand. Strong peaks at 1498, 1444, 1354, 952, and 852 cm⁻¹ in precursor compounds represent the stretching of BO_3 in borate and in-plane-binding of B (OH).[24] When the disulfide bond was linked to the primary amine and changed into a secondary amine, a featured peak showed up at 1141 cm⁻¹. Also, a weak broad peak at 438 cm⁻¹ was assigned to C−N−C stretching, and N−H deformation at 736 cm⁻¹ was identified to

prove the primary amine's transformation into a secondary amine. Two medium peaks at 605 and 636 cm⁻¹ were assigned to the C−S stretching, confirming the presence of dithiocarbamate.

DLS studies revealed an increasing average hydrodynamic diameter from 35.7 nm (bare Au NPs) to 47.3 nm (B-DDTC Au NPs). Due to the bias diffusion, DLS results reflect the average diameter of nanoparticles in solutions. Further nanoparticle size analysis using SEM confirmed that bare and B-DDTC Au NPs had comparable sizes with an average diameter of 6.53 and 11.04 nm, respectively (Figure 3a). Obviously, despite the introduction of reactive groups, B-DDTC Au NPs remained inactive and formed a stable colloidal solution due to the presence of borate protection. The slightly increased particle diameter in B-DDTC Au NPs indicated successful modifications on the Au NP surfaces. However, different from bare Au NPs with an absorption maximum at a wavelength of 530 nm, the adhesive Au NP absorption maximum showed a broad peak at 558 nm (Figure 3b). The 28 nm redshift was due to the surface property changes of the Au NPs with the binding of bidentate ligands (B-DDTC). When the disulfur group was bound to the surface of the Au NPs, due to the coupled plasmon absorbance of NPs in close contact, the bond stabilized the metal's energy level and
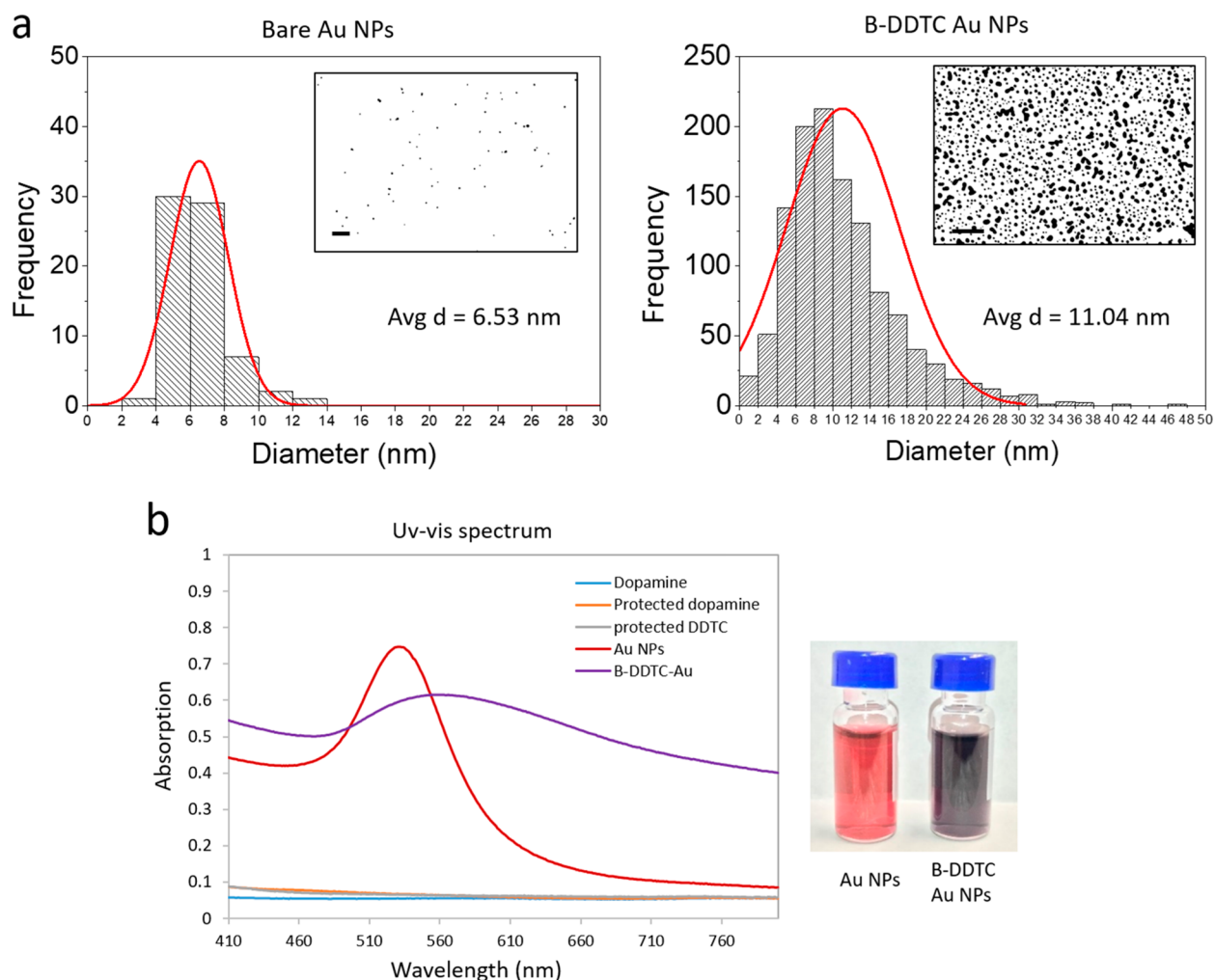
a

b

Figure 3. (a) Statistic histogram plot of the particles size analysis of bare Au NPs coating surface (left) and B-DDTC Au NPs coating surface (right). The binary SEM images of bare Au NP coating and B-DDTC Au NP coating were set in the plots. (b) UV−vis spectrum (left) and images of bare and adhesive Au NP stable suspensions (right).

increased the dielectric constant that induced the plasmonic wavelength redshift. Visually, a color change can be observed from red (bare Au NPs) to purple (adhesive Au NPs).

Surface Coating Using Adhesive Au NPs and Coating Stability Test. We conducted surface coating of adhesive Au NPs and compared it with those of bare Au NPs and DDTC-Au NPs (Figure 4a). The SEM images were taken from multiple areas on each sample; the images shown in the figure indicate the most featured surface morphology. Bare Au NPs demonstrated a very low density of attachment through simple immersion. In the presence of DDTC ligand, Au NPs became adhesive but formed severe aggregations in the colloidal solution due to the interparticle self-polymerization, leading to uneven and dense Au NP coating. On the contrary, borate protected the interparticle reactions caused by catechol groups and thus prevented Au NPs from forming nondispersible aggregates in colloidal solutions. Once borate protection was removed at acidic pH, the activated adhesive Au NPs interacting with surfaces became the predominant reaction because of the polymerization of DDTC ligand and the large nanoparticle surface areas. Interparticle reaction in colloidal solution was limited and only occurred at high Au NP concentrations. Therefore, we were able to achieve evenly coated surfaces by using B-DDTC Au NPs (demonstrated in Figure 4b). It should

be noted that in addition to Au NP concentrations, conditions of the coating process like incubation time and solution agitation can also be used to control interparticle reactions. As a result, adhesive Au NPs can be used to create surfaces with limited and tunable Au NP aggregation. We saw Au NP islands with two to five Au NPs in the SEM image of B-DDTC Au NP coated surfaces (Figure 4a), and the coating was evenly distributed.

We know that the reaction between the catechol groups slows down at acidic pH and in the presence of organic solvents.[23] For further controlled interparticle reaction, we selected a mixed solvent (H_2O/EtOH = 3:7) for surface coating. The coating efficiency was also increased because the DDTC ligand oxidation can be easily activated in water and tends to attach to the surfaces along with the connected Au NP, which creates the driving force of surface coating even to nonreactive materials. The coatings on materials including PS (24-well plates), PET (film), PP (centrifuge tube), and glass (borosilicate) were tested (Figure 5a). As we had expected, the borate protected adhesive Au NPs demonstrated universal reactivity to all materials, and we obtained Au NP evenly coated surfaces. Au NP concentrations and reaction time mainly controlled the Au NP coating density. High concentrations and prolonged incubation time led to high Au NP coating density. Solution agitation also played a role because of catechol
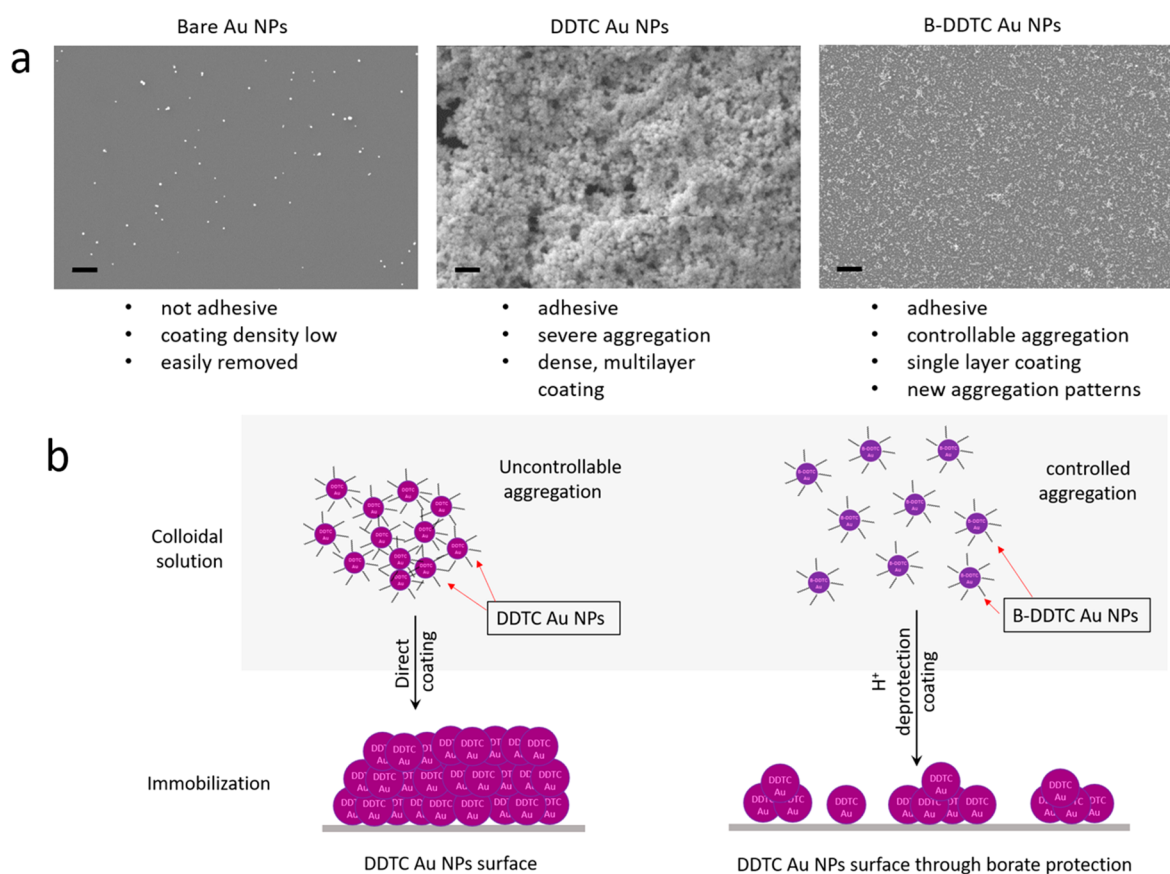
Figure 4. (a) SEM of bare Au NP, DDTC-Au NP, and B-DDTC-Au NP coated surfaces with the same particle concentration (1.97 mg/L) by simple immersion after 24 h (scale bar = 400 nm). (b) Comparison of DDTC-Au NP (left) and borate protected DDTC-Au NP (right) mediated surface adhesion. Borate protected DDTC-Au NPs lead to even and controlled surface coating.

oxidation in the presence of oxygen. Slightly higher Au NP coating density was usually observed at the liquid/air interface if the coating reactions were conducted without proper solution agitation. By using it as an advantage of adhesive Au NPs, we achieved a ring coating in test tubes by using two nonmiscible solvents as shown in Figure 5b. On the macro scale, the coating was well distributed and demonstrated a dark purple color, which was confirmed by UV−vis spectrum and SEM analysis (Figure 5c,d). We observed a broader and longer wavelength UV peak (centered in 650 nm) compared to those of the adhesive Au NPs ligand in solutions (Figure 3b) because of the interparticle reactions during the coating process to form small Au NP aggregates as shown in SEM images (Figure 5d).

To check the application conditions in which these adhesive Au NPs coated surfaces are stable, we tested coating layer stability in water solutions with different pH values and different salt (NaCl) concentrations as well. We chose PET as the substrate surface due to its optical property that made it possible to quantify the result using UV−vis absorption measurement. The results are shown in Figure 6.

From the Figure 6 data, after submersion in water for 24 h in different conditions, coatings on the surfaces kept their thicknesses and densities compared to the nontreated control surface both under different pH (from 4 to 10) and different salt concentrations treatments. The adhesive Au NP coating retained its stability due to the DDTC ligand adhesive property make the coating more durable. These results allow us to apply the coated surfaces under various conditions in aqueous solution.

Removal of Dopamine Shell to Achieve Naked Au NP Coating. Besides the easy surface coating and the good water stability, adhesive Au NPs as described in this study has many other advantages and huge application potentials. For example, surface-enhanced Raman spectroscopy (SERS)[25−27] has been used in the analysis of trace chemicals or identification of biological samples.[28−30] Modifications of Au NPs and/or material surfaces are essential for surface immobilization of Au NPs in SERS. Chemicals introduced into the system may have negative impacts and create noise background and thus reduce SERS sensitivity.[31]

To explore wide applications of adhesive Au NPs, we had tried to remove the DDTC ligands on the Au NPs surface using oxygen plasma treatment. By controlling plasma treatment time and powers, we succeeded in removing the DDTC ligand without detaching Au NPs (Figure 7). From the SEM image, we saw the disappearance of the blurry top surface of self-polymerized DDTC component on Au NP after the oxygen plasma treatment (Figure 7a). The elemental analysis of immobilized Au NPs also confirmed the conclusion. It should be noted that Au NPs coated surfaces after oxygen plasma treatment gave a sharp UV peak (Figure 7b) which was very close to the UV peak of bare Au NPs (Figure 7c). Since the plasma treatment only removed DDTC ligands from Au NPs without affecting Au NPs distribution on surfaces, it indicates that the broad UV peak belongs to the functionalized Au NPs coating itself instead of the aggregation of Au NPs. Because of the removal of DDTC ligands after plasma treatment, we
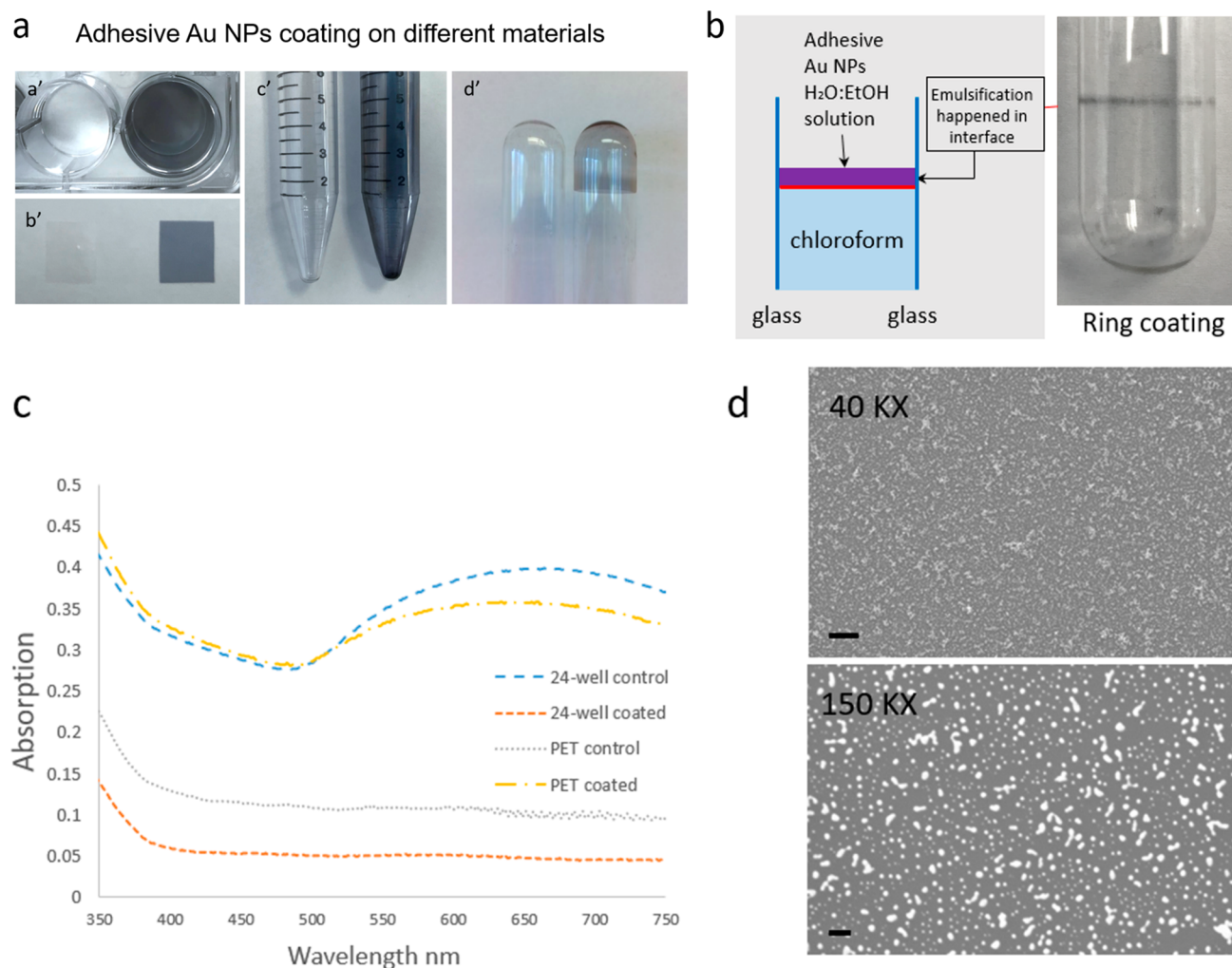
Figure 5. Images of adhesive Au NPs coating surfaces with all images with control (left) and coated surfaces (right). (a) (a′) 24-well plates (polystyrene), (b′) PET films (polyethylene terephthalate), (c′) centrifuge tubes (polypropylene), (d′) glass. (b) Manipulated surface coating using adhesive Au NPs. (c) UV−vis spectra of PET and 24-well plate with adhesive Au NP coating. (d) SEM images of adhesive Au NP coated silicon wafer surfaces with 40 KX (scale bar = 400 nm) and 150 KX (scale bar = 100 nm) of magnification after oxygen treatment for 1 min at 80 W.
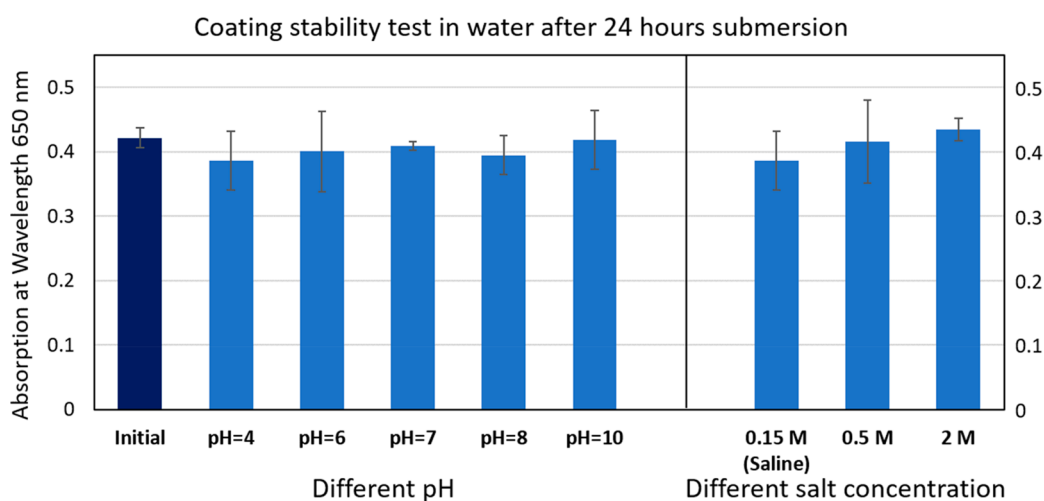

Figure 6. UV−vis absorption of adhesive Au NP coated PET surfaces after 24 h in (a) different pH (pH from 4 to 10). (b) Different NaCl concentrations in water. The absorption was measured at the wavelength of 650 nm, which was the plasmon peak of the coated surfaces. The end point measurement was taken at three spots on the surfaces to ensure accuracy.

obtained a clean and very neat Raman spectrum for Au NP coated surface (Figure 7c).

Formation of "Hot Spots" in SERS. We know that small Au NPs are beneficial for organic molecules to interact with the
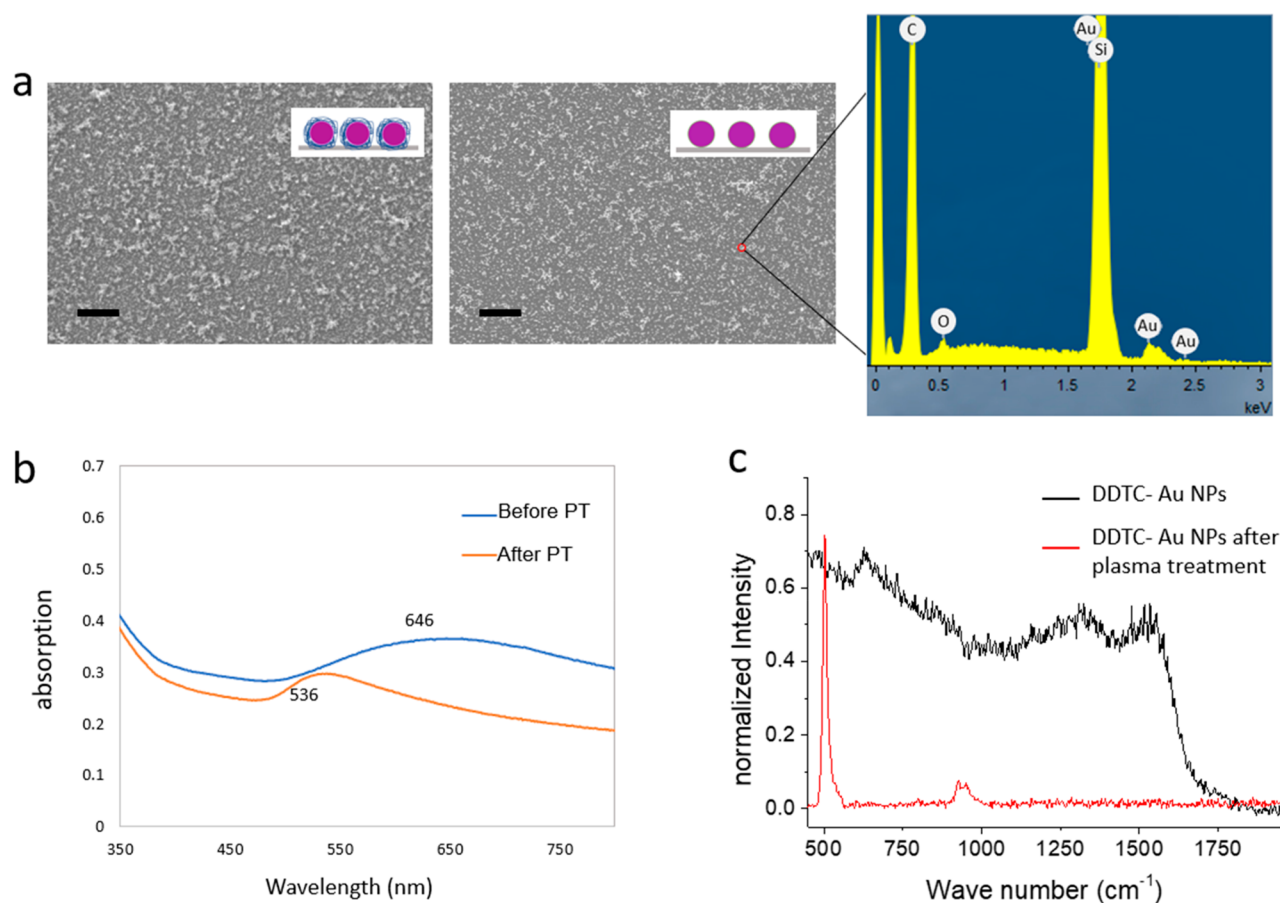
Figure 7. (a) SEM of adhesive Au NP coated surfaces before (left) and after (right) oxygen plasma treatment (scale bar = 400 nm). Organic components on Au NP surfaces were removed after being plasma treated as illustrated in the insets. (b) UV−vis spectra of adhesive Au NP coated PET films before and after oxygen plasma treatment. (c) Raman spectra comparison of adhesive DDTC-Au NP coated surface before and after oxygen plasma treatment. (normalized with silicon featured peak 520 cm^{-1}).

localized gold surface plasmons. Theoretically, the multilayer coating of Au NPs could provide more "hot spots" in more complex 3D structures to increase the sensitivity of SERS detection. Now it is generally accepted that Au NP aggregates with 2−3 particles will give outstanding SERS signals.[32,33] Because of the intramolecular interactions between the borate functional groups,[34] borate protection led to the formation of loosely connected Au NPs in colloidal solutions which facilitate the formation of moderate 3D aggregates with 2−5 Au NPs when the borate is removed under acidic condition. Therefore, we conducted SERS studies on adhesive Au NP coated surfaces by using R6G as a model analyst. Characteristic Raman peaks of R6G are at 1651, 1603, 1510, 1572, 1363, 1312, 1184, 771, and 611 cm^{-1}.[4,35−37] We observed most of the major R6G peaks at 1 × 10^{-6} M concentration on adhesive Au NP treated surfaces, indicating a SERS signal boost by a factor of 10^4 in comparison with naked Au NPs (Figure 8a,b). By using electron energy loss spectroscopy (EELS) studies to map nanoparticle surface plasmon resonances,[38−41] we confirmed that the trimer's pointy end provided hotspots and did the most enhancement work on the SERS signals (Figure 8c). It should be noted that the signal at 1572 cm^{-1} (twisting vibration mode of phenyl group) was less intense than that at 1603 cm^{-1} (the vibration mode vertical to the xanthene ring) at lower R6G concentration, suggesting that the R6G molecules adsorbed on the trimer Au NP aggregations were rather vertically oriented toward their surfaces at low concentrations.[42,43]

To further investigate the "hot spots" concept, we extended our study to high density and especially multilayer Au NP coated surfaces by using the advantages of adhesive Au NPs (Figure 9). Interestingly, none of these high density and multilayer coatings presented better SERS signals. From the SEM images and the SERS data, we believe that the dense multilayer coating aggregation, in general, did form a rough metallic surface, with the increased particle junctions for a stronger electromagnetic coupling.[44] However, we should also realize that the Au NPs we used in the study were very small (less than 10 nm) in size. Therefore, there is a good chance that Au NP aggregates observed might have been tightly packed and did not have enough void space to form the real "hot spots". In fact, this proves that medium size Au NPs are required in order to form rough surfaces for good SERS signals.[33] Further fundamental and applied studies on adhesive metallic (Ag and Au) NP applications in SERS as well as others are underway.

■ SUMMARY AND CONCLUSIONS

In contrast with the common coating strategy of pretreating a target substrate to make it suitable for Au NP coating, this study focused on Au NP modification. We have developed a novel method to produce adhesive Au NPs for easy and effective coating on nonpretreated surfaces. Such adhesive Au NPs were colloidal stable when protected with borate and can be easily activated after deprotection to achieve good coating surfaces. This method lends increased versatility to Au NP applications in
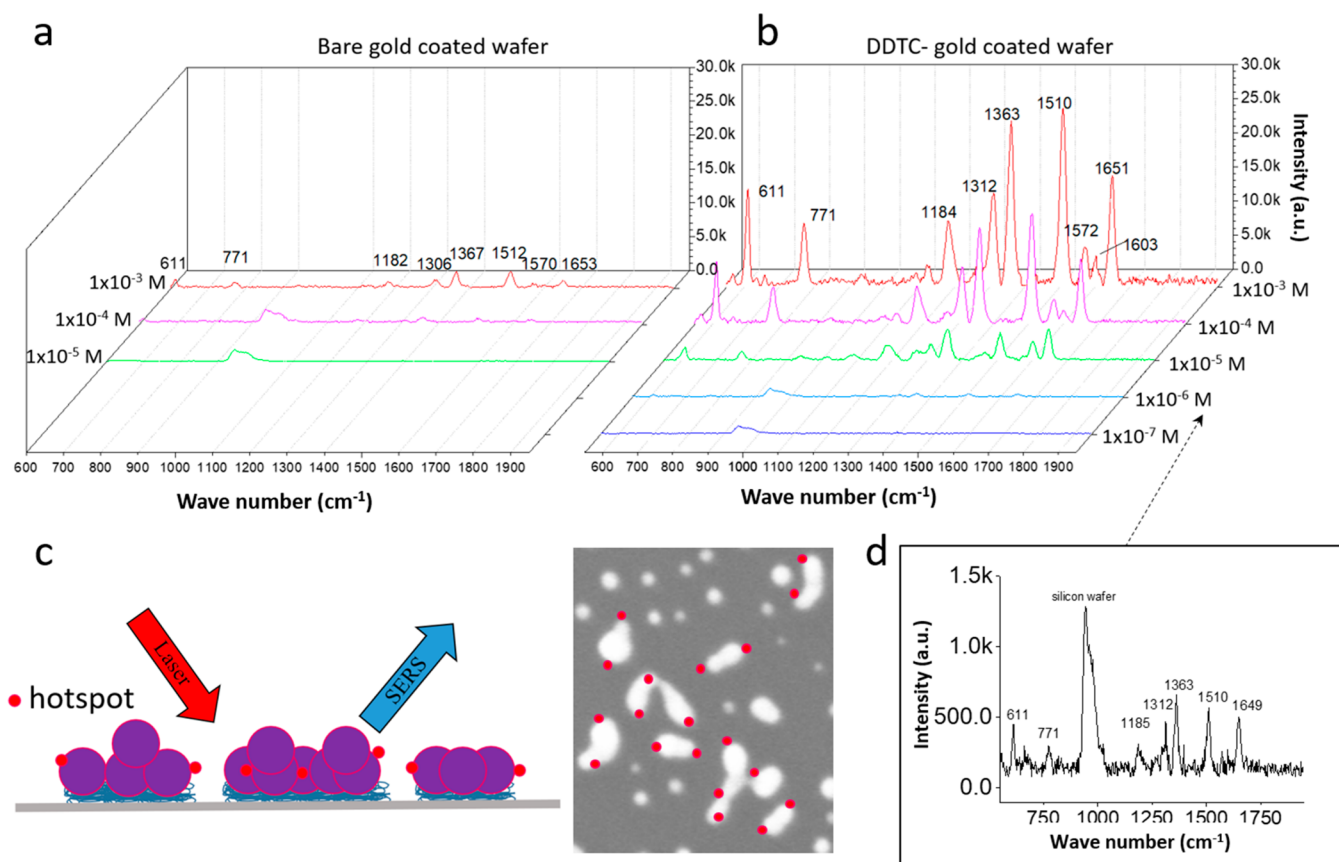
Figure 8. Raman spectra of rhodamine 6G (R6G) on naked (a) and adhesive (b) Au NP treated silicon wafers. All Raman spectra were performed with 20s acquisition time (2s × 10 times). (c) SERS signal enhancement demonstration. (d) Zoomed in SERS spectrum of DDTC-Au coated silicon wafer with the concentration of 1×10^{-6} M.
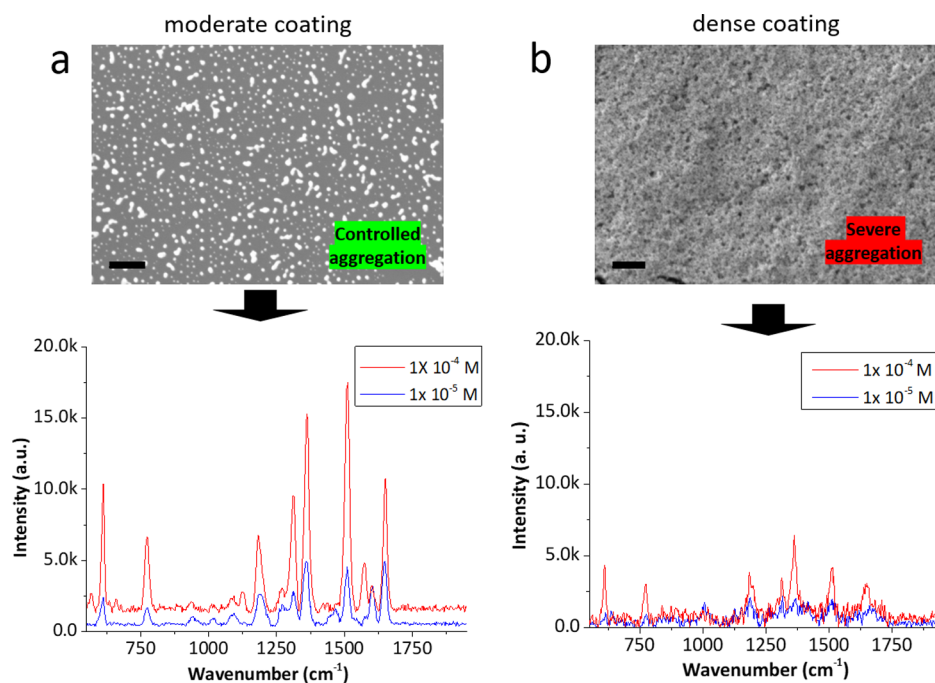

Figure 9. SEM images (scale bar = 200 nm) and Raman spectra of SERS detection of (a) the moderately coated surfaces and (b) the densely coated surfaces. All coating was performed with the same adhesive Au NPs and coating protocol. Surfaces were treated with oxygen plasma before SERS signal acquisition.

basic and applied sciences. In addition, through borate protection, the adhesive Au NPs allow us to manipulate Au NP self-assembly and aggregation degrees for wide applications.

■ AUTHOR INFORMATION

Corresponding Author
*Tel:1-201-216-5640. Fax: 1-201-216-8240. E-mail: jliang2@ stevens.edu.

ORCID
Tianchi Liu: 0000-0002-1435-7233
Fan Yang: 0000-0002-5074-568X
Xing Wang: 0000-0002-9990-1479

Notes
The authors declare no competing financial interest.

■ REFERENCES

(1) Saha, K.; Agasti, S. S.; Kim, C.; Li, X.; Rotello, V. M. Gold Nanoparticles in Chemical and Biological Sensing. *Chem. Rev.* **2012**, *112*, 2739−2779.

(2) Chen, Y. P.; Xianyu, Y. L.; Jiang, X. Y. Surface Modification of Gold Nanoparticles with Small Molecules for Biochemical Analysis. *Acc. Chem. Res.* **2017**, *50*, 310−319.

(3) Priyadarshini, E.; Pradhan, N. Gold Nanoparticles as Efficient Sensors in Colorimetric Eetection of Toxic Metal Ions: A Review. *Sens. Actuators, B* **2017**, *238*, 888−902.

(4) Nie, S. M.; Emery, S. R. Probing Single Molecules and Single Nanoparticles by Surface-Enhanced Raman Scattering. *Science* **1997**, *275*, 1102−1106.

(5) Krug, J. T.; Wang, G. D.; Emory, S. R.; Nie, S. M. Efficient Raman Enhancement and Intermittent Light Emission Observed in Single Gold Nanocrystals. *J. Am. Chem. Soc.* **1999**, *121*, 9208−9214.

(6) Rodriguez-Lorenzo, L.; Alvarez-Puebla, R. A.; García de Abajo, F. J.; Liz- Marzan, L. M. Surface Enhanced Raman Scattering Using Star-shaped Gold Colloidal Nanoparticles. *J. Phys. Chem. C* **2010**, *114*, 7336−7340.

(7) Alvarez-Puebla, R. A.; Agarwal, A.; Manna, P.; Khanal, B. P.; Aldeanueva-Potel, P.; Carbó-Argibay, E.; Pazos-Pérez, N.; Vigderman, L.; Zubarev, E. R.; Kotov, N. A.; Liz-Marzán, L. M. Gold Nanorods 3D-supercrystals as Surface Enhanced Raman Scattering Spectroscopy Substrates for the Rapid Detection of Scrambled Prions. *Proc. Natl. Acad. Sci. U. S. A.* **2011**, *108*, 8157−8161.

(8) Li, J. F.; Huang, Y. F.; Ding, Y.; Yang, Z. L.; Li, S. B.; Zhou, X. S.; Fan, F. R.; Zhang, W.; Zhou, Z. Y.; Wu, D. Y.; Ren, B.; Wang, Z. L.; Tian, Z. Q. Shell-isolated Nanoparticle-Enhanced Raman Spectroscopy. *Nature* **2010**, *464*, 392−395.

(9) Bodelon, G.; Montes-Garcia, V.; Lopez-Puente, V.; Hill, E. H.; Hamon, C.; Sanz-Ortiz, M. N.; Rodal-Cedeira, S.; Costas, C.; Celiksoy, S.; Perez-Juste, I.; Scarabelli, L.; La Porta, A.; Perez-Juste, J.; Pastoriza-Santos, I.; Liz-Marzán, L. M. Detection and Imaging of Quorum sensing in Pseudomonas Aeruginosa Biofilm Communities by Surface-enhanced Resonance Raman Scattering. *Nat. Mater.* **2016**, *15*, 1203−1211.

(10) Burda, C.; Chen, X. B.; Narayanan, R.; El-Sayed, M. A. Chemistry and Properties of Nanocrystals of Different Shapes. *Chem. Rev.* **2005**, *105*, 1025−1102.

(11) Daniel, M. C.; Astruc, D. Gold Nanoparticles: Assembly, Supramolecular Chemistry, Quantum Size-related Properties, and Applications Toward Biology, Catalysis, and Nanotechnology. *Chem. Rev.* **2004**, *104*, 293−346.

(12) Homola, J. Surface Plasmon Resonance Sensors for Detection of Chemical and Biological Species. *Chem. Rev.* **2008**, *108*, 462−493.

(13) Njoki, P. N.; Lim, I. I. S.; Mott, D.; Park, H. Y.; Khan, B.; Mishra, S.; Sujakumar, R.; Luo, J.; Zhong, C. J. Size Correlation of Optical and Spectroscopic Properties for Gold Nanoparticles. *J. Phys. Chem. C* **2007**, *111*, 14664−14669.

(14) Huang, J.; Zhang, L. M.; Chen, B.; Ji, N.; Chen, F. H.; Zhang, Y.; Zhang, Z. J. Nanocomposites of Size-controlled Gold Nanoparticles and Graphene Oxide: Formation and Applications in SERS and Catalysis. *Nanoscale* **2010**, *2*, 2733−2738.

(15) Brown, K. R.; Walter, D. G.; Natan, M. J. Seeding of Colloidal Au Nanoparticle Solutions. 2. Improved Control of Particle Size and Shape. *Chem. Mater.* **2000**, *12*, 306−313.

(16) Yang, F. K.; Zhao, B. X. Adhesion Properties of Self-polymerized Dopamine Thin Film. *Open Surf. Sci. J.* **2011**, *3*, 115−122.

(17) Lee, H.; Scherer, N. F.; Messersmith, P. B. Single-molecule Mechanics of Mussel Adhesion. *Proc. Natl. Acad. Sci. U. S. A.* **2006**, *103*, 12999−13003.

(18) Lee, H.; Dellatore, S. M.; Miller, W. M.; Messersmith, P. B. Musselinspired Surface Chemistry for Multifunctional Coatings. *Science* **2007**, *318*, 426−430.

(19) Liebscher, J.; Mrówczyński, R.; Scheidt, H. A.; Filip, C.; Hădade, N. D.; Bende, A.; Beck, S. Structure of Polydopamine: A Never-Ending Story? *Langmuir* **2013**, *29*, 10539−10548.

(20) Bisaglia, M.; Mammi, S.; Bubacco, L. Kinetic and Structural Analysis of the Early Oxidation Products of Dopamine: Analysis of the Interactions with Alpha-Synuclein. *J. Biol. Chem.* **2007**, *282*, 15597−15605.

(21) Waite, J. H.; Benedict, C. V. Assay of Dihydroxyphenylalanine (dopa) in Invertebrate Structural Proteins. *Methods Enzymol.* **1984**, *107*, 397−413.

(22) Lee, B. P.; Huang, K.; Nunalee, F. N.; Shull, K. R.; Messersmith, P. B. Synthesis of 3,4-dihydroxyphenylalanine (DOPA) Containing Monomers and their Co-polymerization with PEG-diacrylate to Form Hydrogels. *J. Biomater. Sci., Polym. Ed.* **2004**, *15*, 449−464.

(23) Chen, T. P.; Liu, T. C.; Su, T. L.; Liang, J. F. Self-Polymerization of Dopamine in Acidic Environments without Oxygen. *Langmuir* **2017**, *33*, 5863−5871.

(24) Devi, S. A.; Philip, D.; Aruldhas, G. Infrared, Polarized Raman, and SERS Spectra of Borax. *J. Solid State Chem.* **1994**, *113*, 157−162.

(25) Hamon, C. Colloidal Design of Plasmonic Sensors Based on Surface Enhanced Raman Scattering. *J. Colloid Interface Sci.* **2018**, *512*, 834−843.

(26) Fleischmann, M.; Hendra, P. J.; McQuillan, A. J. Raman Spectra of Pyridine Adsorbed at a Silver Electrode. *Chem. Phys. Lett.* **1974**, *26*, 163−166.

(27) Jeanmaire, D. L.; Van Duyne, R. P. Surface Raman spectroelectrochemistry: Part I. Heterocyclic, Aromatic, and Aliphatic Amines Adsorbed on the Anodized Silver Electrode. *J. Electroanal. Chem. Interfacial Electrochem.* **1977**, *84*, 1−20.

(28) Xu, M. L.; Gao, Y.; Han, X. X.; Zhao, B. Detection of Pesticide Residues in Food Using Surface-Enhanced Raman Spectroscopy: A Review. *J. Agric. Food Chem.* **2017**, *65*, 6719−6726.

(29) Liu, Y.; Zhou, H. B.; Hu, Z. W.; Yu, G. X.; Yang, D. T.; Zhao, J. S. Label and Label-free Based Surface-enhanced Raman Scattering for Pathogen Bacteria Detection: A review. *Biosens. Bioelectron.* **2017**, *94*, 131−140.

(30) Sharma, G.; Deckert-Gaudig, T.; Deckert, V. Tip-enhanced Raman Scattering-Targeting Structure-specific Surface Characterization for Biomedical Samples. *Adv. Drug Delivery Rev.* **2015**, *89*, 42−56.

(31) Skoog, D. A.; Holler, F. J.; Nieman, T. A. Raman Spectroscopy. In *Principles of Instrumental Analysis*; Saunders College: Philadelphia, 1998.

(32) Imura, K.; Okamoto, H.; Hossain, M. K.; Kitajima, M. Visualization of Localized Intense Optical Fields in Single Gold-nanoparticle Assemblies and Ultrasensitive Raman Active Sites. *Nano Lett.* **2006**, *6*, 2173−2176.

(33) Wustholz, K. L.; Henry, A. I.; McMahon, J. M.; Freeman, G. R.; Valley, N.; Piotti, M. E.; Natan, M. J.; Schatz, G. C.; Van Duyne, R. P. Structure-activity Relationships in Gold Nanoparticle Dimers and

Trimers for Surface-enhanced Raman Spectroscopy. *J. Am. Chem. Soc.* **2010**, *132*, 10903−10910.

(34) Kale, S. N.; Mona, J.; Dhobale, S.; Thite, T.; Laware, S. L. Intramolecular and Intermolecular Crosslinked Poly (vinyl alcohol)−borate Complexes for the Sustained Release of Fertilizers and Enzymes. *J. Appl. Polym. Sci.* **2011**, *121*, 2450−2457.

(35) Foyer, C. H.; Halliwell, B. The Presence of Glutathione and Glutathione Reductase in Chloroplasts: A Proposed Role in Ascorbic Acid Metabolism. *Planta* **1976**, *133*, 21−25.

(36) Hildebrandt, P.; Stockburger, M. Surface-enhanced Resonance Raman Spectroscopy of Rhodamine 6G Adsorbed on Colloidal Silver. *J. Phys. Chem.* **1984**, *88*, 5935−5944.

(37) Watanabe, H.; Hayazawa, N.; Inouye, Y.; Kawata, S. DFT Vibrational Calculations of Rhodamine 6G Adsorbed on Silver: Analysis of Tip-enhanced Raman Spectroscopy. *J. Phys. Chem. B* **2005**, *109*, 5012−5020.

(38) Nelayah, J.; Kociak, M.; Stephan, O.; Garcia de Abajo, F. J.; Tence, M.; Henrard, L.; Taverna, D.; Pastoriza-Santos, I.; Liz-Marzán, L. M.; Colliex, C. Mapping Surface Plasmons on a Single Metallic Nanoparticle. *Nat. Phys.* **2007**, *3*, 348−353.

(39) Losquin, A.; Zagonel, L. F.; Myroshnychenko, V.; Rodríguez-González, B.; Tencé, M.; Scarabelli, L.; Förstner, J.; Liz-Marzán, L. M.; García de Abajo, F. J.; Stéphan, O.; Kociak, M. Unveiling Nanometer Scale Extinction and Scattering Phenomena through Combined Electron Energy Loss Spectroscopy and Cathodoluminescence Measurements. *Nano Lett.* **2015**, *15*, 1229−1237.

(40) Guiton, B. S.; Iberi, V.; Li, S.; Leonard, D. N.; Parish, C. M.; Kotula, P. G.; Varela, M.; Schatz, G. C.; Pennycook, S. J.; Camden, J. P. Correlated Optical Measurements and Plasmon Mapping of Silver Nanorods. *Nano Lett.* **2011**, *11*, 3482−3488.

(41) Rodríguez-Lorenzo, L.; Alvarez-Puebla, R. A.; Pastoriza-Santos, I.; Mazzucco, S.; Stéphan, O.; Kociak, M.; Liz-Marzán, L. M.; García de Abajo, F. J. Zeptomol Detection Through Controlled Ultrasensitive Surface-enhanced Raman Scattering. *J. Am. Chem. Soc.* **2009**, *131*, 4616−4618.

(42) Moskovits, M. Surface-enhanced Raman Spectroscopy: A Brief Retrospective. *J. Raman Spectrosc.* **2005**, *36*, 485−496.

(43) Ghosh, S. K.; Pal, T. Interparticle Coupling Effect on the Surface Plasmon Resonance of Gold Nanoparticles: From Theory to Applications. *Chem. Rev.* **2007**, *107*, 4797−4862.

(44) Ngo, Y. H.; Li, D.; Simon, G. P.; Garnier, G. Effect of Cationic Polyacrylamides on the Aggregation and SERS Performance of Gold Nanoparticles-treated Paper. *J. Colloid Interface Sci.* **2013**, *392*, 237−246.